Variations in Seafloor Depth Estimates Under Different Swath-width Characteristics of Submarine Structures in the California Borderlands

University of Washington
School of Oceanography
Senior Thesis 2016

Jessica Zannakis

Jessica Zannakis
(Advisor: Miles Logsdon)

School of Oceanography
University of Washington
1503 NE Boat Street
Seattle, WA 98105
jzannaki@uw.edu

keywords: multibeam, rugosity, Crespi Knoll

ABSTRACT

The California Continental Borderland region off the coast of Southern California is home to many types of geological features on the seafloor (aka. submarine structures) that have resulted from movement along tectonic plate boundaries. Crespi Knoll, a submarine structure in this area, formed as a gentle restraining bend in association with movement along the Palos Verdes master fault. This study used Crespi Knoll as the canvas on which to experiment with the technology aboard the R/V Thomas G. Thompson from 06-07 February 2016. Depth measurements were collected using the Kongsberg EM302, and were used to compare acquisition modes of the multibeam while paring beam spacing (Equiangle, Equidistance) with beam angle (50º, 60º, 70º) in 5-minute intervals at 4 knot survey increments. Multibeam sonar backscatter was post-processed with CARIS HIPS (ver. 9.1) in both 5 meter and 25 meter resolutions, and spatial surface rugosity was calculated in ArcGIS (ver. 10.3.1). Much variation occurred in the depth estimates when comparing a single survey line of unchanging multibeam acquisition settings to one with changing settings. The unchanging acquisition settings consistently produced deeper depth estimates, and the rugosity increased using the 5m resolution surface data as the finer resolution accounted for the small-scale variations of depth at the seafloor.

INTRODUCTION

Crespi Knoll is a submarine structure found within the California Continental Borderlands (Figure 1), lying 31.37 miles off the coast of Southern California and 29.23 miles southeast of Santa Catalina Island. Crespi Knoll is classified as a gentle restraining bend associated with the larger Palos Verdes master fault, and has been active since the Quaternary period (Mann 2007). It is also the merging site of the San Pedro Basin Fault Zone and the Catalina Fault Zone, which together form the San Diego Trough Fault Zone at a pull-apart basin to the east of Crespi Knoll (Legg et al. 2002).

The California Continental Borderlands formed during the Neogene period development of the Pacific-North America transform plate boundary, and is filled regionally with many restraining and releasing bend structures along several of the major strike-slip right-lateral faults in this area (Legg et al. 2007). A restraining bend structure, like the one that formed Crespi Knoll, results from the "concentration of regional maximum compressive stress on pre-existing, basement[1] fault trends in stable cratonic[2] areas" with the "periodic release of these bend-related stress concentrations one of the leading causes of intraplate earthquakes within otherwise stable cratons" (ie. 1986 Oceanside earthquake in Southern California) (Mann 2007).

In general terms, Crespi Knoll can be thought of as a mound or pop-up that has formed on the end of a pull-apart basin as the compressive stresses have compressed the rock together to generate uplift. Due to the extreme uplift, Miocene volcanic rocks have been dredged from Crespi Knoll indicating a possible reactivation of an ancient extensional structure formed in the Inner Borderland region (Legg et al. 2007).

1 Basement: harder and usually older igneous and metamorphic rocks that underlie the main sedimentary rock sequences of a region and extend downward to the base of the crust (USGS Earthquake glossary)

2 Cratonic/craton: the stable interior portion of a continent characteristically composed of ancient crystalline basement rock (Encyclopaedia Britannica)

The preservation of the morphology of these Borderland restraining-bend pop-ups is due to the low erosion rates of deep offshore basins that surround them (Legg et al. 2007).

Crespi Knoll served as our main study area as we utilized the hydrographic survey technology available aboard the R/V Thomas G. Thompson, specifically the multibeam sonar system (MBSS) Kongsberg EM302 multibeam by Kongsberg Maritime Int. The purpose of the MBSS for this study is to gather variations of seafloor depth estimates using different swath-width characteristics and to use these estimates to calculate the seafloor rugosity ("roughness") of Crespi Knoll. Rugosity is a dimensionless ratio but can be thought of as the "roughness" due to the small-scale variations of height/depth at the seafloor.

The Kongsberg EM302 is designed to do mapping from 10m to 7,000m depth, with swath-widths up 5.5x water depth to a max of 8,000m (Kongsberg 2013). Through electronic beam steering the multibeam system is able to compensate for the dynamic motion (roll, pitch, yaw) of the vessel (up to 15^o, 10^o, and 10^o respectively) while maintaining constant geometry of its surroundings on the seafloor (Kongsberg 2013, Llewellyn).

Changing the beam spacing and the beam width of the MBSS can be expected to give equal meter distance between depth points on the seafloor ("equidistant") or ensures that all beams sent from the MBSS have equal angular spacing and a higher density of soundings closer to the center of the survey line ("equiangle"), respectively (Kongsberg 2013). It can be expected that the higher density of soundings below the boat while using equiangle beam spacing will result in more accurate depth estimates of the seafloor directly beneath the boat than further out towards the edge for a given swath. However, equidistant beam spacing will provide more accurate depth estimates along the entire swath-width as it reduces "missed" points on the seafloor. Using both equidistant beam spacing with an increasing beam width is expected to result in higher rugosity as there will likely be more accurate data for a larger area to calculate rugosity.

METHODS

The R/V Thomas G. Thompson set sail from San Diego Harbor in San Diego, California, for a 2 day cruise from 06-07 February 2016, and transited to Crespi Knoll, our main study site, which lies approximately 29.23 miles southeast of Santa Catalina Island and approximately 31.37 miles off the coast of California.

Preplanning for the cruise, including route, study site location, and location of survey lines and CTD (Conductivity, Temperature, and Density) casts, was completed by Dr. Miles Logsdon of the University of Washington School of Oceanography who also accompanied those attending this research cruise. CTD casts were used to collect salinity, temperature, and depth data in order to create Sound Velocity Profiles (SVPs) accounting for the variations in the speed of sound through seawater due to stratification of the water column.

The Kongsberg EM302 aboard the Thompson was used to collect depth estimates of the seafloor during the entire duration of the cruise upon exiting San Diego Harbor. Once we reached our main survey site at Crespi Knoll we performed multiple surveys with overlapping, parallel track lines directly above Crespi Knoll and the surrounding areas. The Kongsberg EM302 was operated at a frequency 30Khz and the boat speed was approximately 4 knots. Each survey line ran for approximately 30 minutes and covered 2 miles straight-line distance.

For the purposes of this study we used data from two interior survey lines, from here on out known as survey lines A and B. Swath-width (beam width and beam spacing) was held constant on survey line A (50^o beam, equidistant). Settings on the multibeam were changed during survey line B on 5 minute intervals for a total of 25 minutes (initially set to 50^o equidistance then changing to 50^o equiangle, 60^o equiangle, 60^o equidistance, 70^o equidistance, 70^o equiangle) in order to vary the swath-width.

The raw multibeam soundings were imported into CARIS HIPS software (ver. 9.1) to form base surfaces in both 5 meter and 25 meter resolutions. The base-surface construction created in CARIS utilized the CUBE (Combined Uncertainty and Bathymetry Estimator) algorithm, which generates "point-wise estimates of depth from dense surroundings" (Vásquez 2007). These base surfaces were then exported to the ESRI ArcGIS (ver. 10.3.1) software, a geographic information system, to create 5m and 25m resolution raster data layers. The 5m resolution allows for more possible variation in the depth estimates as opposed to the 25m resolution that averages more depth values gathered for a given area due to the greater area coverage per grid cell.

Seafloor surface swath images were created in ArcGIS to show both survey lines used (Figure 2) and the overlap area of each swath (Figure 3). In this overlap area of the desired swaths, 5 locations were picked at approximate equal distance intervals within each 5-minute time interval of swath-width changes. The depths from each swath at these locations were recorded and used to compare variance between the depth estimates due to beam geometry altered by changes to beam width settings on the multibeam (ie. constant beam width of 50^o and equidistant beam spacing of survey line A vs 60^o equidistant beam of survey line B). This was done for both the finer- and coarser-scale 5m and 25m resolutions respectively.

Comparing the depth estimates from each survey line was done using a "subtractive" or differencing method of depths that calculates the "differential effect," or amount of change, from a treatment after placed on a "treatment group" versus the "control group" in the same natural setting. Survey line A is our "control group" as the swath-width remained constant, while survey line B represents the "treatment group" with its varying multibeam acquisition settings. This is a fairly simple way to compare depth estimates derived using different acquisition settings from the same geo-referenced bathymetric base surface.

Percent error calculations were made as another way to compare the depth estimates taken from the data. Percent relative error is calculated using equations 1 and 2 below, with "experimental" values representing depth estimates from survey line B and the "known" values from survey line A. The difference of percent error (*equation 3*) was used in this study to calculate the range of values of percent error for each acquisition setting change, as well as for each major beam width (degrees) change. Finally, total percent error represents the sum of percent error values (*equation 4*) to calculate total error for each major beam width change.

1. $error = (experimental - known) \times -1$
2. $\% \text{ error} = \frac{error}{known} \times 100\%$
3. $\text{diff \% error} = \text{largest \% error} - \text{smallest \% error}$
4. $\text{total \% error} = \text{sum \% error}$

Rugosity calculations were made possible after utilizing the Surface Volume (3D Analyst) tool in ArcGIS to measure the

two components (3-dimensional and 2-dimensional surface areas) of the rugosity equation. The equation compares the 3-D surface area to the 2-D surface area, in this case the 3-D and 2-D areas of the overlap of our two survey lines.

$$rugosity = \frac{area\ (3\text{-}D)}{area\ (2\text{-}D)}$$

The 3-D surface area represents the actual surface area in its measurement accounting for the changes in depth, while the 2-D surface area is the flat, geometric surface area. The closer the rugosity value is to one means the 3-D and 2-D surface areas are nearly equal indicating that the surface is area is very smooth. Likewise a value much greater than 1 indicates a surface that is very rough. In this study the rugosity values of the 5m resolution and 25m resolution data are compared to see which produces a "more rough" surface.

RESULTS

The comparison of depth estimates under different acquisition beam widths is best represented in Tables 1 and 2, which depict all depth estimates and difference calculations (diff = survey line A - survey line B) made at the geographic locations selected from the overlapping area of the survey lines (Table 1), as well as error and percent relative error calculations made from the depth estimates (Table 2). The normalized depth estimates for each survey line were included as well in the last two columns on Table 1. When looking at both 5m and 25m resolution depth estimates, survey line A consistently produced deeper estimates than survey line B.

The largest difference under 5m resolution occurred during the first 5 min interval (70^o EA) with a value of 4.561m. The smallest difference under 5m resolution occurred during the third interval (60^o ED) with a value of 0.431m, and the next closest during that same interval of 0.713m. The average differences in order of intervals were 3.941m (70^o EA), 3.740m (70^o ED), 1.925m (60^o ED), 2.742m (60^o EA), 2.435m (50^o EA), and 1.650m (50^o ED). All estimates under EA beam spacing produced a larger average estimate than their counterparts (ie. 70^o ED vs 70^o EA). The average depth estimate differences for the three major changes in degrees of beam width were as follows: (70^o) 3.841m, (60^o) 2.334m, and (50^o) 2.042m.

Depth estimates under 25m resolution produced the largest difference of 7.091m during the second interval (70^o ED), and the smallest difference of 0.325m in the third interval (60^o ED). The average differences in order of intervals were 5.894m (70^o EA), 5.779 (70^o ED), 2.510m (60^o ED), 3.751m (60^o EA), 2.056m (50^o EA), and 1.837m (50^o ED). The EA beam spacing for 60^o and 50^o beam widths produced larger averages of differences than ED for 60^o and 50^o respectively, however the 70^o EA average difference was smaller than 70^o ED. In order of largest to smallest average differences, including both ED and EA, were 5.684m (70^o), 3.062m (60^o), and 1.946m (50^o).

Expanding on Table 1, the estimates from all locations were normalized to values between 0-1 and plotted (Figure 4) as a 1:1 ratio with survey line A values on the x-axis and those of survey line B with the changes in swath-width on the y-axis. As the depths have been normalized and plotted in this fashion allowed comparison of the depths as a ratio of survey line A to survey line B. A line of y=x was also drawn on each plot to show where the 1:1 ratio of depth estimates would fall. All values fell below this line no matter the change in swath-width.

Percent error calculations (Table 2) resulted in the greatest difference or range of

percent error from 5m resolution to be 0.451% (60^o ED) and smallest value of 0.055% (70^o ED), when judged on each change in acquisition settings on the multibeam. The greatest range of percent error when judged by change of beam width (major degree changes) came from 60^o beam with a value of 0.451%. Meanwhile the smallest value came from 70^o beam at 0.174%. 25m resolution data showed slightly different results.

The greatest range of percent error for each change in acquisition settings came from 60^o ED with a value of 0.880%, and the smallest value from 70^o EA at 0.114%. Comparing major changes in beam width (degree changes), the smallest range percent error value was 0.295% (50^o) and the largest was 0.880% (60^o). In order of smallest to largest total percent error for both 5m and 25m resolution data is 50^o, 60^o, 70^o.

The 2-D and 3-D areas from 5m resolution were calculated to be 14,345,759.523m^2 and 14,653,677.149m^3. 25m resolution 2-D and 3-D areas were calculated both much higher at 16,399,838.402m^2 and 16,447,753.305m^3. From these values rugosity was calculated for both 5m and 25m resolution with each value resulting in a number greater than 1. The rugosity value from 5m resolution data was greater than that of 25m resolution data (1.021 vs 1.003).

DISCUSSION/CONCLUSION

The use of modern multibeam sonar systems, such as the Kongsberg EM302, in hydrographic surveying, whether for creation of nautical charts or scientific research, relies upon methods that reduce the induced error in gridded depth estimates. This study evaluated the error that resulted in the selection of different beam width (affecting actual swath-width) and beam spacing (equiangle or equidistance) during data acquisition.

From the scatter plots (Figure 4) we see that all normalized depth values fell below the y=x 1:1 reference line. This indicates that the depth estimates at each location (for both 5m and 25m resolution) were greater when taken from survey line A, with unchanging swath-width characteristics. As a whole, both 70^o and 60^o beam widths with 5m resolution data produced the smallest variation at all geographic locations from which depth estimate values were recorded as each value fell very close to the 1:1 reference line.

The trendlines/lines of best fit for both 70^o EA and 70^o ED fall on nearly the same location on the graph which suggests that although the actual depth values may not be the same, there was little to no variation of the resulting ratio of depths from each survey line between these two acquisition settings. The graph of depth estimates from 70^o under 25m resolution data shows that the depth estimates gathered from both EA and ED followed similar trends as indicated by their nearly parallel trendlines.

Studying just the lines of best fit, the most variation occurred from the 25m resolution data under 60^o and 50^o beam widths as the lines intersect. This indicates very different trends of the ratio of normalized depth values from survey line A to those of survey line B. The individual values vary widely, too, in their proximity to the lines of best fit and the 1:1 reference line, which further supports the idea of a wide range of the ratios of depth values from survey line A to survey line B at the individual locations (unlike the parallel lines of best fit mentioned above for 5m resolution 70^o and 60^o).

After calculation of all average differences of depths it is apparent that these values can only give a very basic

representation for what happened when changing swath-width, thus why the percent error calculations were added. More specifically, the range of percent error values allows for more in-depth comparison of the variance of depth estimates between each acquisition setting change as well as each major beam width (degrees) change. The larger the range of percent error, the more variation of values given the acquisition settings.

Studying 5m resolution data the 70^{o} beam width overall held the smallest value of range of percent error, while for 25m resolution data the 50^{o} beam width settings held the smallest range of percent error. Thinking big picture, the smallest range of percent error values mean these data can be considered the "most consistent" data as they showed little variation throughout.

When conducting hydrographic surveying, changes in acquisition settings will be made to accommodate the depth of the seafloor or seafloor features that are being studied (ie. wider beam for a wider swath when travelling over shallow features vs narrower beam needed for greater depths as each beam reaches further to hit the seafloor). Finding acquisition settings that produce the smallest range of % error allows for potentially easier and more precise calculations of depth to then be made.

FIGURES/TABLES

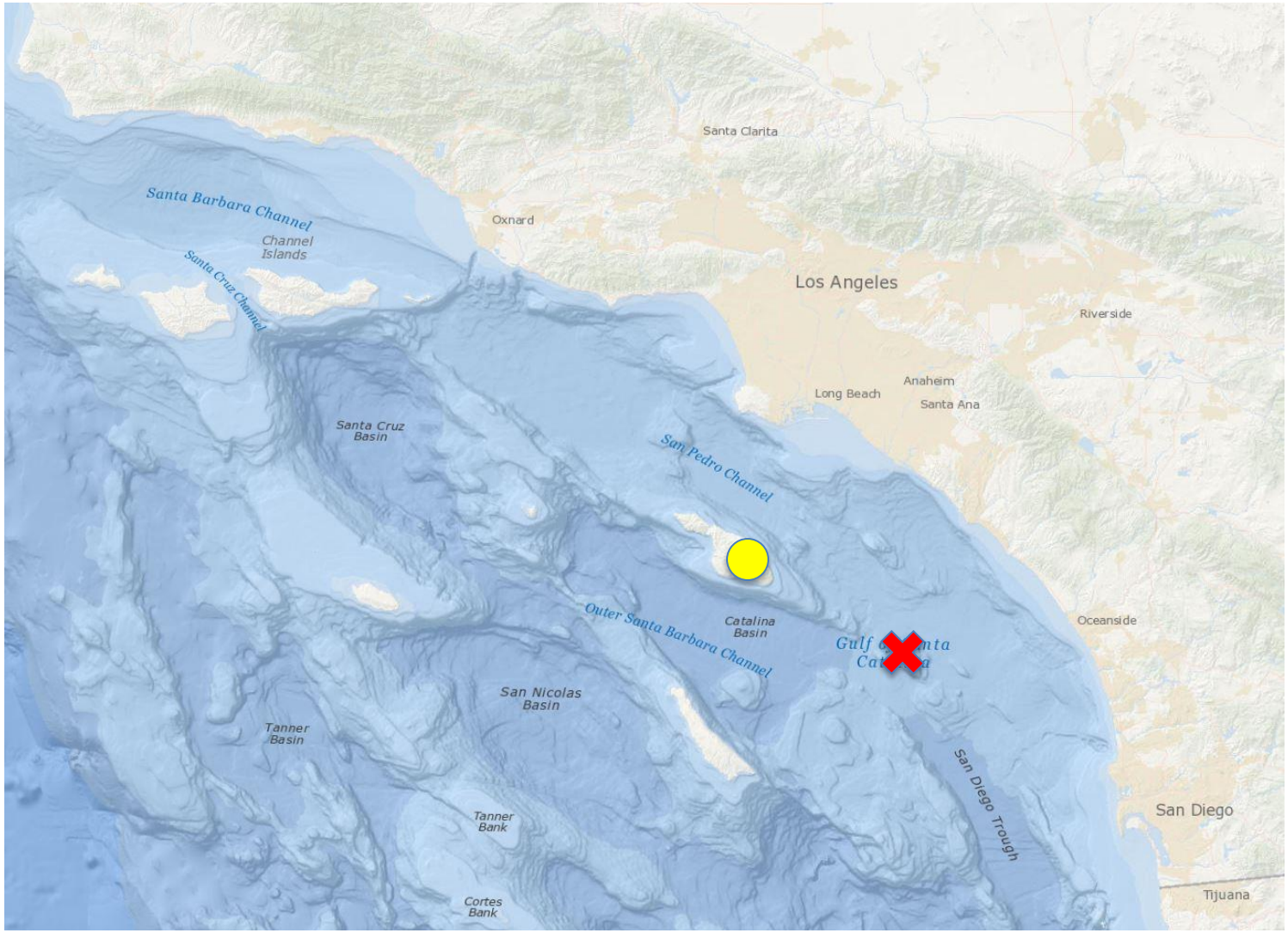

Figure 1 California Continental Borderlands off the coast of Southern California. Crespi Knoll (red 'x'). For reference, Crespi Knoll lies 31.37 miles off the coast of Southern California and 29.23 miles southeast of Santa Catalina Island (yellow circle).

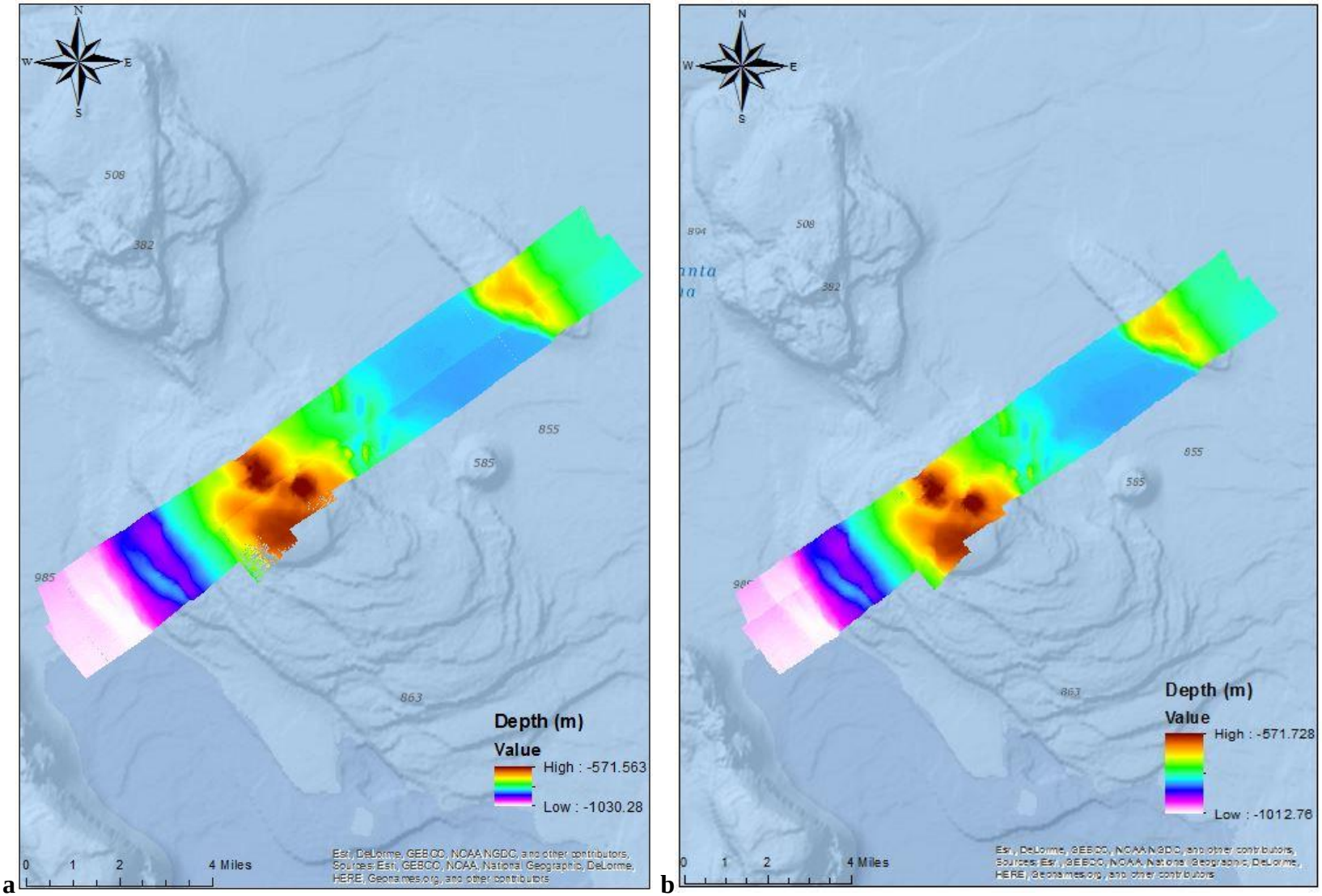

a b

Figure 2a, 2b Swath surface images corresponding to survey lines created through multibeam data
(a) 5m resolution (b) 25m resolution

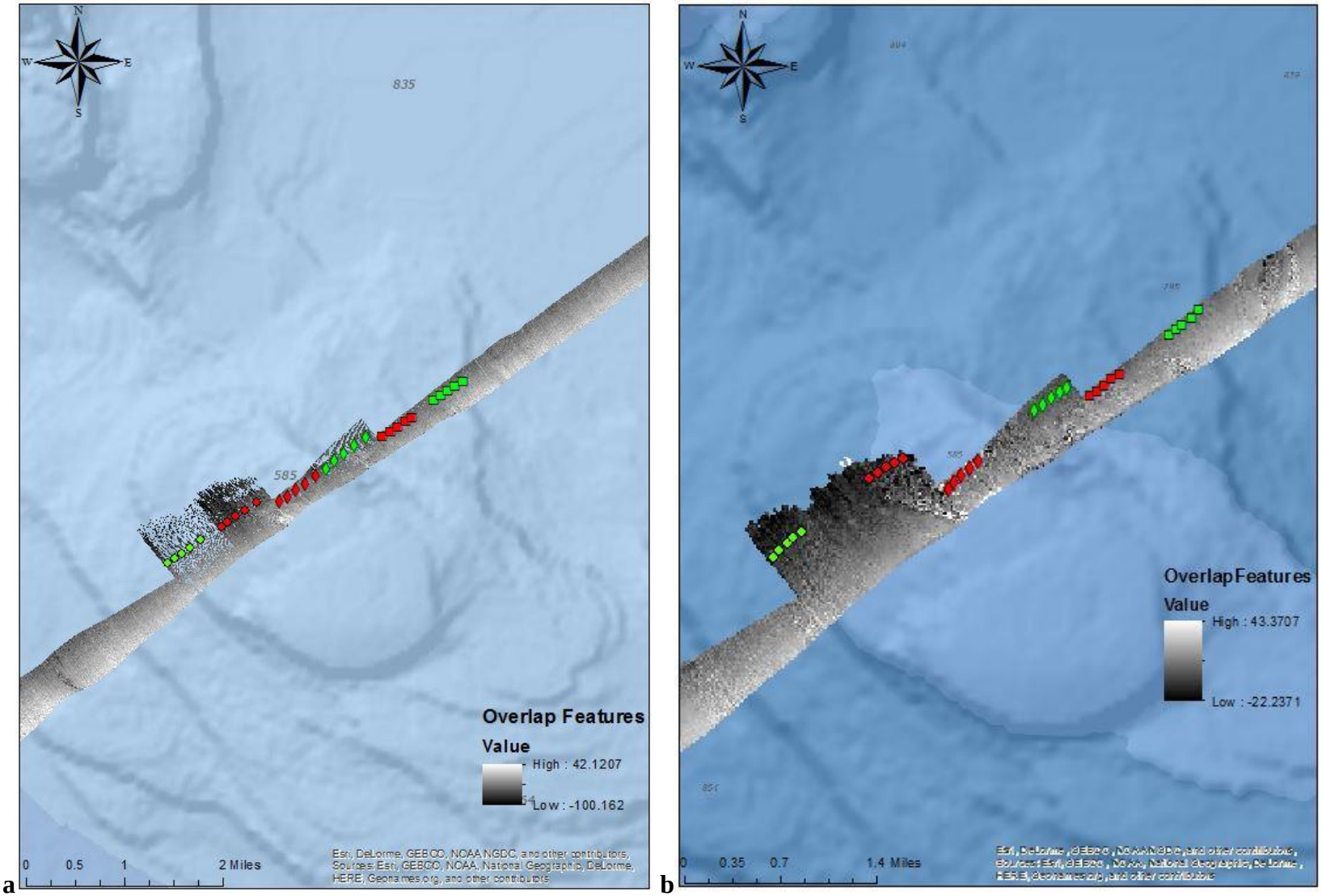

a b

Figure 3a, 3b Overlap of individual swaths created from corresponding survey lines and geographic locations used to gather depth estimates. Widest overlap region corresponds to 70^{o} beam (circles), then 60^{o} (diamonds), and finally 50^{o} (squares)
(a) 5m resolution (b) 25m resolution

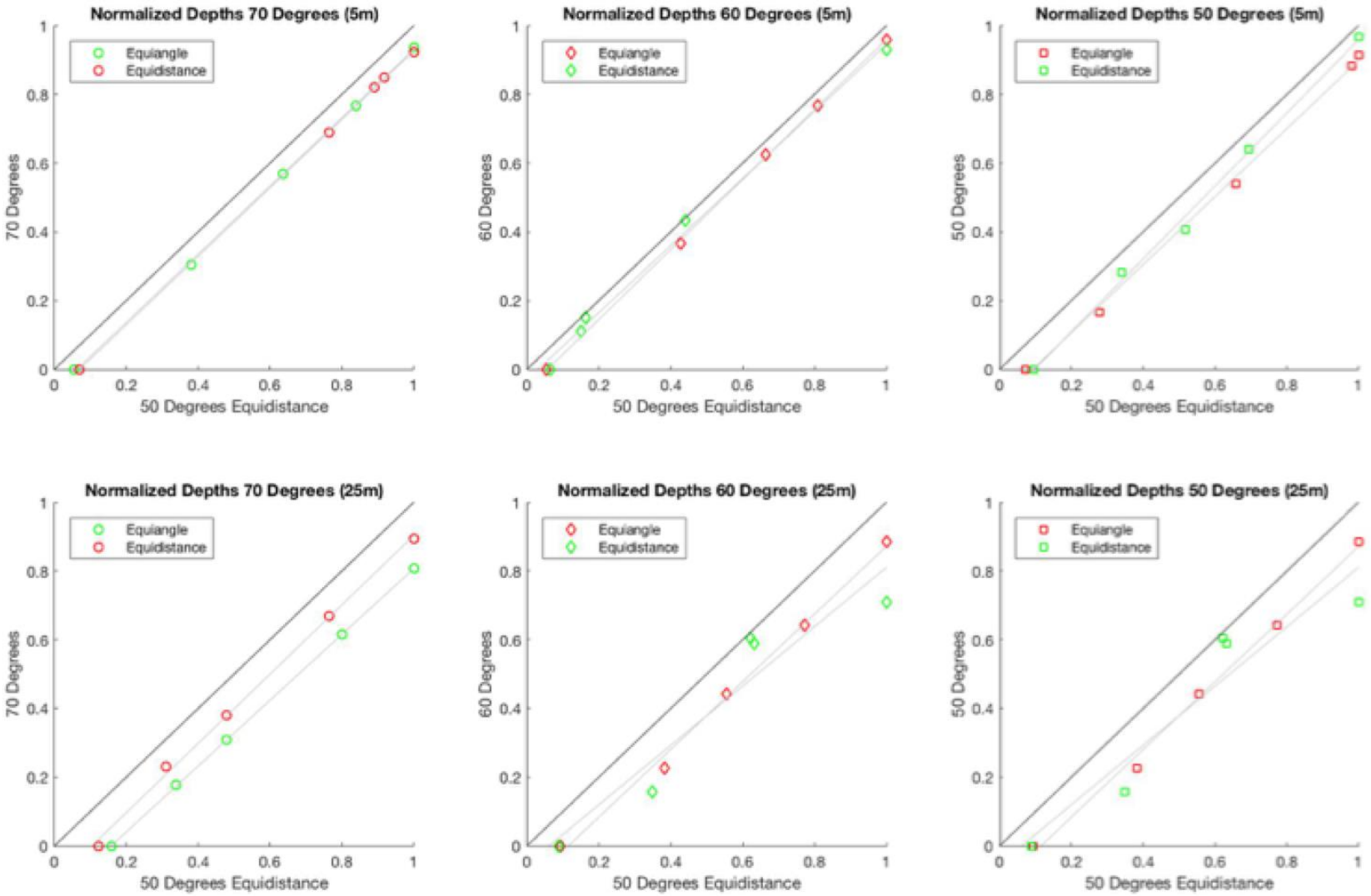

Figure 4 Plots showing the normalized depths of survey lines A and B for each change of swath-width settings (both degree changes and ED vs EA). Survey line A (swath with constant settings of 50° ED) shown on x-axis of each plot. All values consistently below straightline y=x on each plot showing that survey line A produced deeper depth estimates for each case.

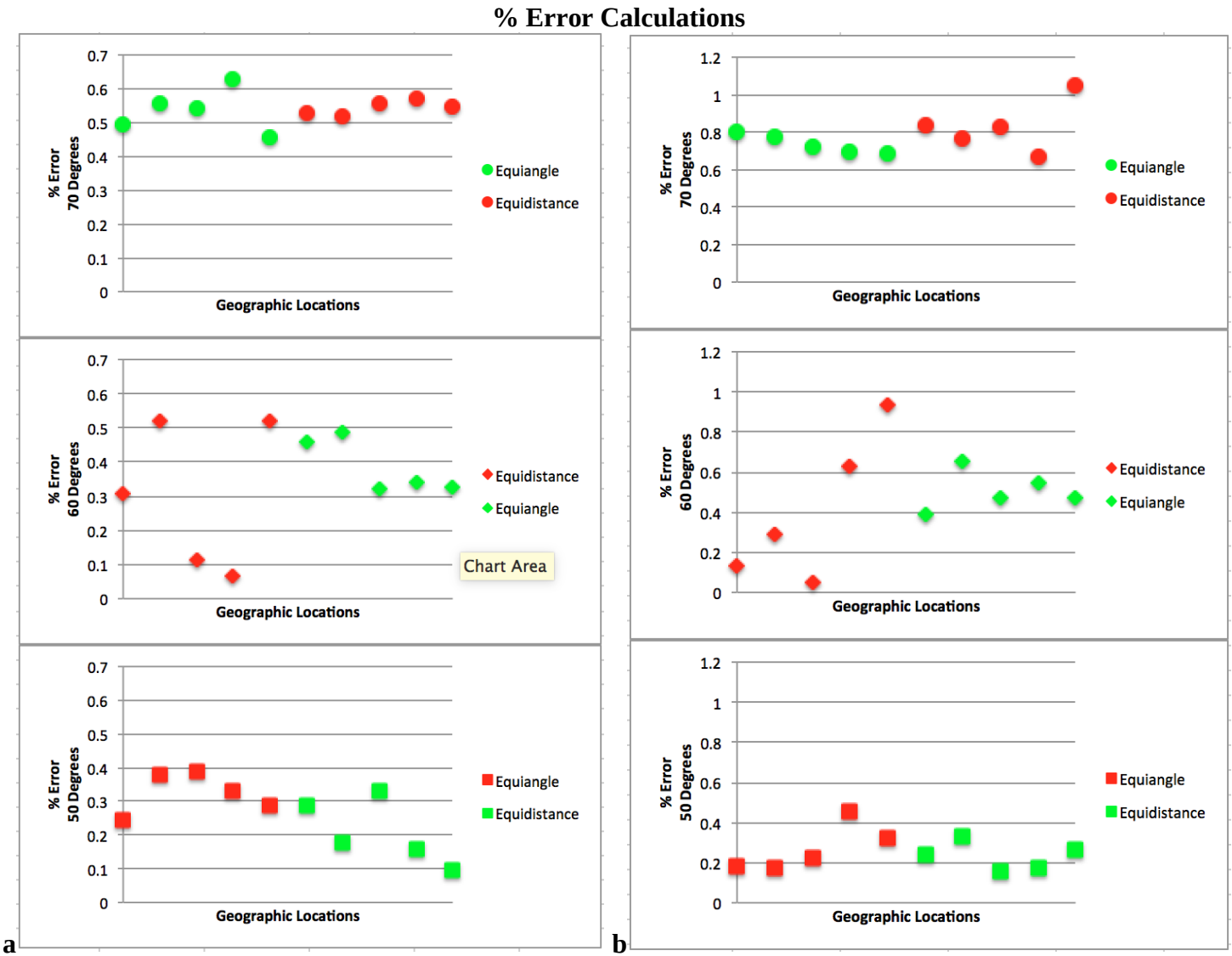

Figure 5a, 5b Percent error calculations separated by 5m and 25m resolution data, and plotted against their corresponding geographic locations labeled appropriately according to acquisition settings.
(a) 5m resolution (b) 25m resolution

		5m						25m					
Swath	Point #	Depth (A)	Depth (B)	Differences	Avg. Diff.	Norm. (A)	Norm. (B)	Depth (A)	Depth (B)	Differences	Avg. Diff.	Norm. (A)	Norm. (B)
70° EA	1	760.094299	756.33197	3.762329	3.9408812	1	0.93668386	773.581543	767.392578	6.188965	5.5894164	1.22697649	1.12282256
	2	750.492126	746.330017	4.162109		0.83840527	0.76836124	767.176453	761.221191	5.955262		1.11918539	1.01896444
	3	738.52179	734.518005	4.003785		0.63695678	0.56957718	756.8302	751.367371	5.462829		0.94506856	0.85313475
	4	723.293396	718.731995	4.561401		0.38067852	0.30391482	752.373901	747.157349	5.216552		0.87007361	0.78228439
	5	703.887756	700.672974	3.214782		0.05410149	0	746.623474	741.5	5.123474		0.77329982	0.687077
70° ED	6	695.232178	691.573425	3.658753	3.7404908	0.8908372	0.81976726	723.597656	717.555664	6.041992	5.77926	1.61850702	1.48676186
	7	696.675293	693.067078	3.608215		0.91886918	0.84878092	710.033081	704.592407	5.440674		1.32273253	1.20409906
	8	700.85199	696.937988	3.914002		1	0.92397194	693.702209	687.968445	5.733764		0.96663915	0.84161487
	9	688.750549	684.802795	3.947754		0.76493392	0.68825024	683.975891	679.387085	4.588806		0.75455754	0.65449899
	10	652.944702	649.370972	3.57373	**3.840686**	0.0694184	0	673.261169	666.170105	7.091064	**5.6843382**	0.52092387	0.36630378
60° ED	11	615.370972	613.473022	1.89795	1.9250004	0.14930828	0.1107675	614.315063	613.478027	0.837036	2.5104982	0.12786643	0.11086913
	12	611.190735	608.01825	3.172485		0.06442217	0	603.513733	601.755737	1.757996		-0.0914711	-0.1271699
	13	616.093689	615.380981	0.712708		0.16398416	0.14951153	614.09845	613.773804	0.324646		0.12346777	0.11687534
	14	629.730408	629.299133	0.431275		0.44089862	0.43214092	608.694153	604.86084	3.833313		0.01372525	-0.064116
	15	657.263489	653.852905	3.410584		1	0.93074287	621.634644	615.835144	5.7995		0.27650173	0.158734
60° EA	16	679.370972	676.244324	3.126648	2.7422608	0.05454125	0	712.956421	710.16394	2.792481	3.75058025	0.6404059	0.59169386
	17	700.716736	697.299255	3.417481		0.42689681	0.36728226	721.792542	717.061218	4.731324		0.79454322	0.71200999
	18	714.358032	712.049622	2.30841		0.66485561	0.6245877	727.072083	723.625183	3.4469		0.88663954	0.82651181
	19	722.655212	720.19104	2.464172		0.80959163	0.76660661	733.715088	729.683472	4.031616		1.00252014	0.93219262
	20	733.570618	731.176025	2.394593	**2.3336306**	1	0.95822871	740.593628	737.084045	3.509583	**3.06164578**	1.1225094	1.06128823
50° EA	21	735.844971	734.049255	1.795716	2.435071	0.07160836	0	739.472412	738.152039	1.320373	2.055859	0.21626102	0.16360807
	22	741.013	738.220337	2.792663		0.27769555	0.16633161	742.346924	741.03949	1.307434		0.33088888	0.2787519
	23	750.522034	747.618591	2.903443		0.65689043	0.54110888	749.536865	747.833557	1.703308		0.61760452	0.54968115
	24	758.691284	756.175415	2.515869		0.98265831	0.88233217	762.744995	759.290955	3.45404		1.14430948	1.00657158
	25	759.12616	756.958496	2.167664		1	0.91355935	766.24884	763.7547	2.49414		1.28403346	1.18457381
50° ED	26	777.134338	774.911926	2.222412	1.6496582	0.09508861	0	783.358887	781.474731	1.884156	1.8370852	0.36141355	0.28079763
	27	782.873169	781.491577	1.381592		0.34063151	0.28151841	784.750732	782.184143	2.566589		0.42096533	0.31115069
	28	787.016296	784.395874	2.620422		0.51790026	0.4057823	786.913696	785.672668	1.241028		0.51351039	0.46041149
	29	791.142273	789.8927	1.249573		0.69443522	0.64097072	793.24646	791.849426	1.397034		0.78446544	0.72469163
	30	798.283936	797.509644	0.774292	**2.0423646**	1	0.96687097	802.6698	800.573181	2.096619	**1.9464721**	1.18765455	1.09794814

Table 1 Both 5m and 25m resolution depth estimates for survey lines A and B, and calculations for differences of depth estimates, average differences (averages for swath-width degree changes shown in bold), and the normalized depths of survey lines A and B.

	5m			25m		
Swath	%Error	Diff.%Error	Total%Error	%Error	Diff.%Error	Total%Error
70° EA	0.49498187	0.17392526	5.40220938	0.80004042	0.11382117	7.82960435
	0.55458397			0.77625714		
	0.54213499			0.72180378		
	0.63064325			0.69334569		
	0.45671799			0.68621925		
70° ED	0.52626347	0.05525698		0.83499331	0.38233948	
	0.51791919			0.76625641		
	0.55846342			0.82654544		
	0.57317617			0.67090172		
	0.54732506	**0.17392526**		1.0532412	**0.38233948**	
60° ED	0.30842371	0.45058062	3.46906625	0.13625516	0.88007803	4.58773747
	0.51906628			0.29129345		
	0.11568176			0.05286546		
	0.06848566			0.62976012		
	0.51890666			0.9329435		
60° EA	0.46022691	0.16456752		0.39167625	0.26382013	
	0.4877122			0.65549638		
	0.32314468			0.47407954		
	0.34098862			0.54947977		
	0.32642979	**0.45058062**		0.47388782	**0.88007803**	
50° EA	0.24403455	0.14282191	2.67526457	0.17855609	0.27672165	2.52287972
	0.37687099			0.1761217		
	0.38685646			0.22724806		
	0.33160642			0.45284335		
	0.28554727			0.3255		
50° ED	0.28597527	0.23596195		0.24052271	0.16934959	
	0.17647712			0.32705787		
	0.33295651			0.15770827		
	0.15794542			0.17611601		
	0.09699456	**0.2898619**		0.26120567	**0.29513508**	

Table 2 Percent error calculations from depth estimates at each point separated by 5m and 25m resolution data. Differences of % error calculated to show the range of % error values for each swath-width acquisition setting (range of values for swath-width degree changes shown in bold). Total error calculated for each degree change.

	2D Area	3D Area	Rugosity
5m	14345759.522501	14653677.148528	1.02146402
25m	16399838.401697	16447753.304773	1.00292167

Table 3 5m resolution and 25m resolution 2-D area and 3-D area of the overlap of survey lines A and B. Rugosity of 5m resolution greater at 1.021 vs 25m resolution at 1.003.

REFERENCES

Earthquake Glossary - Basement. USGS.

Craton. Encyclopaedia Britannica Online.

Kongsberg. 2013. *EM302 30Khz multibeam echo sounder*. Kongsberg Maritime AS.

Kongsberg. 2013. *EM Sector Coverage Beam Spacing modes*. Kongsberg Maritime AS.

Legg, Mark R., and Chris Goldfinger. 2002. *Earthquake potential of major faults offshore southern California: collaborative research with Oregon State University and Legg Geophysical*. ResearchGate. Report number: 01HQGR0018.

Legg, Mark R., C. Goldfinger, M. J. Kamerling, J. D. Chaytor, and D. E. Einstein. 2007. *Morphology, structure and evolution of California Continental Borderland restraining bends*. Geological Society 290:143-168. doi:10.1144/SP290.3

Llewellyn, Kristian C. 2006. *Corrections for beam pattern residuals in backscatter imagery from the Kongsberg-Simrad EM300 multibeam echosounder.* University of New Brunswick (Canada), ProQuest Dissertations Publishing.

Mann, P. 2007. *Global catalogue, classification and tectonic origins of restraining and releasing bends on active and ancient strike-slip fault systems*. Geological Society 290:13-142. doi:10.1144/SP290.2

Vásquez, Miguel E. 2007. *Tuning the CARIS implementation of CUBE for Patagonian Waters*. The University of New Brunswick (Canada), Department of Geodesy and Geomatics Engineering.